

# Spontaneous surface magnetization and chiral Majorana modes in the $p \pm is$ superconductors

Wang Yang, Chao Xu, and Congjun Wu

*Department of Physics, University of California, San Diego, California 92093, USA*

Majorana fermions are often proposed to be realized by first singling out a single non-degenerate Fermi surface in spin-orbit coupled systems, and then imposing boundaries or defects. We take a different route starting with two degenerate Fermi surfaces without spin-orbit coupling. By the method of “boundary of boundary”, both the zero energy Majorana modes and the dispersive chiral ones are formed in superconducting systems with the mixed  $p \pm is$  pairings. Their surfaces develop spontaneous magnetizations with directions determined by the boundary orientations and the phase difference between the  $p$  and  $s$ -component gap functions. Along the magnetic domain walls on the surface, the chiral Majorana modes propagate unidirectionally, which can be controlled by external magnetic fields. The surface magnetization is a magneto-electric effect which can be analyzed based on the Ginzburg-Landau free energy analysis.

PACS numbers:

Majorana fermions are their own anti-particles which were first introduced to high energy physics<sup>1</sup>. In the past decade, they have been intensively investigated in the context of condensed matter physics<sup>2</sup>. The braiding of Majorana particles exhibits non-Abelian statistics<sup>3-6</sup>, which is distinct from the usual Fermi and Bose statistics. The braiding and fusion rules can be applied for quantum computations<sup>7-11</sup>. The topological nature of Majorana modes makes the braiding and fusion robust from the decoherence process which is detrimental to the realization of quantum computers.

There have been a great deal of interests in realizing Majorana fermions. In the  $\nu = \frac{5}{2}$  fractional quantum Hall state, Majorana fermions emerge as fractional quasi-particle excitations<sup>3</sup>. Majorana bound states were proposed to exist on boundaries, in vortex cores, and in defects of topological superconducting systems. In one dimension, Majorana modes emerge on edges of the  $p$ -wave spinless superconducting wires<sup>12</sup>. In two dimensions, they exist in vortex cores of the spinless  $p_x + ip_y$  superconductors<sup>13</sup>, in those of topological superconducting surfaces due to the proximity effect<sup>14,15</sup>, and in half-quantum vortex cores of the spinful chiral  $p$ -wave superconductors<sup>5,16</sup>. They also appear at point defects in three dimensional topological superconductors<sup>17</sup>. The interaction effects in Majorana fermions have also been discussed by various authors<sup>18-20</sup>. Recent experiments have provided evidence to the existence of Majorana zero modes and chiral Majorana fermions in condensed matter systems<sup>21-23</sup>.

A Majorana fermion is half of a usual fermion in view of the degrees of freedom that they contain. Since electrons have two spin degrees of freedom, the chiral Majorana fermions can only be obtained by a “half of half” method. Typically, the first “half” is achieved by singling out a non-degenerate Fermi surface in spin-orbit coupled systems, which becomes effectively single-component. The second “half” is performed by imposing boundaries or defects to generate zero modes.

On the other hand, there have been considerable inter-

ests in studying superconducting states with mixed singlet and triplet pairings. A spontaneously time-reversal symmetry breaking mixing is preferred energetically exhibiting  $\pm \frac{\pi}{2}$  phase difference between the gap functions in these two different channels<sup>24</sup>. This class of novel pairing states have been proposed in the ultra-cold electric dipolar fermion systems<sup>24</sup>, in cold fermion systems under the  $p$ -wave Feshbach resonances<sup>25</sup>, in the iron-pnictide superconductors<sup>26</sup>, and in the inversion symmetry breaking superconducting systems<sup>27</sup>. The spontaneous time reversal symmetry breaking leads to gapped Dirac cones on the surface with nontrivial gravitational responses and thermal Hall effects<sup>27-33</sup>. Furthermore, competing  $s$  and  $p$ -wave pairing instabilities may play an important role in the superconducting states observed in  $\text{Cu}_x\text{Bi}_2\text{Se}_3$ <sup>31</sup>,  $\text{Sn}_{1-x}\text{In}_x\text{Te}$ <sup>31</sup>, and  $\text{Cd}_2\text{Re}_2\text{O}_7$ <sup>27</sup>.

In this article, we analyze the formation of the chiral Majorana fermions in superconductors with the mixed singlet and triplet pairing symmetry of the  $p \pm is$  type. Different from previous works, there are two degenerate Fermi surfaces in the absence of spin-orbit coupling. The strategy “half of half” is implemented as “boundary of boundary”. We show that the boundaries of  $p \pm is$  superconductors are spontaneously magnetized, and the magnetization are opposite for  $p \pm is$  pairings. The domain wall between the  $p \pm is$  superconducting regions on the surface is actually also a magnetization domain wall, along which a chiral Majorana mode propagates unidirectionally. These Majorana fermions can be controlled by external magnetic fields. We also show that the spontaneous surface magnetization is a manifestation of the magnetoelectric effect based on a Ginzburg-Landau free energy analysis.

When the pairing strengths in the  $p$  and  $s$ -channels are nearly degenerate, their mixing leads to the time-reversal symmetry breaking pairing pattern  $p \pm is$ <sup>24</sup>. The corresponding gap function matrix reads  $\Delta_{\alpha\beta}(\vec{k}) = \Delta_s(\vec{k})(i\sigma_2)_{\alpha\beta} + \Delta_p(\vec{k})\hat{d}(\vec{k}) \cdot (i\vec{\sigma}\sigma_2)_{\alpha\beta}$  where  $\hat{d}(\vec{k})$  is a unit real vector and  $\vec{\sigma}$ 's are the Pauli matrices in spin space.

Only when the phase difference between  $\Delta_s$  and  $\Delta_p$  equals to  $\pm\frac{\pi}{2}$ ,  $\Delta_{\alpha\beta}$  is proportional to a unitary matrix. Typically, unitary pairings are energetically more favorable over non-unitary ones<sup>34</sup>. Both time reversal ( $T$ ) and inversion ( $P$ ) symmetries are spontaneously broken in the  $p \pm is$  pairing states. Nevertheless, the system is invariant up to an overall phase under the  $PT$ -transformation, *i.e.*, the combined parity and time-reversal operations.

For simplicity, we start with a 1D  $p_z \pm is$  superconductor, whose Bogoliubov-de Gennes (BdG) Hamiltonian reads

$$H_{1d} = \frac{1}{2} \int dz \psi^\dagger(z) \left( \left( -\frac{\hbar^2}{2m} \partial_z^2 - \mu(z) \right) \tau_3 - \Delta_s \sigma_2 \tau_1 - \frac{\Delta_p}{k_f} (i\sigma_3 \sigma_2) \tau_1 i \partial_z \right) \psi(z), \quad (1)$$

in which  $\psi(z) = (c_\uparrow^\dagger(z) c_\downarrow^\dagger(z) c_\uparrow(z) c_\downarrow(z))^T$ ;  $\tau_i$ 's are the Pauli matrices in the Nambu space;  $k_f$  is the Fermi wavevector;  $\Delta_s$  and  $\Delta_p$  represent the singlet and triplet pairing strengths which can be assumed real without loss of generality. The BdG Hamiltonian Eq. (1) possesses the particle-hole symmetry  $P_h H_{1d} P_h^{-1} = -H_{1d}$  where  $P_h$  is an anti-unitary transformation defined as  $P_h \psi^\dagger(z) P_h^{-1} = \psi^\dagger(z) \sigma_0 \tau_1 K$ , with  $K$  the complex conjugate operation. The triplet pairing pattern in Eq. 1 corresponding to the  $d$ -vector configuration  $\hat{d} \parallel \hat{z}$ , hence the  $z$ -component of spin is conserved represented as  $S_z = \frac{1}{4} \sigma_3 \tau_3$ . In the absence of  $\Delta_s$ , the system preserves the time-reversal symmetry  $T \psi^\dagger(z) T^{-1} = \psi^\dagger(z) i \sigma_2 \tau_0 K$ , and there exists a chiral operator  $C_{ch} = -i T P_h = \sigma_2 \tau_1$  anti-commuting with the Hamiltonian. An open boundary condition is imposed along the  $z$ -direction at the upper ( $z = \frac{L}{2}$ ) and lower ( $z = -\frac{L}{2}$ ) edges, with  $\mu(z) = \frac{\hbar^2}{2m} k_f^2$  at  $|z| < \frac{L}{2}$  and  $\mu(z) = -\infty$  at  $|z| > \frac{L}{2}$ , where  $L$  is the system size.

When  $\Delta_s = 0$ , there exist two Majorana zero modes at each edge of the system. The associated creation operators for the four Majorana modes are  $\gamma_\lambda^{a,\dagger} = \int dz \psi^\dagger(z) \Psi_\lambda^a(z)$ , in which  $a = +(-)$  for upper (lower) edge and  $\lambda = \pm$  labelling the two zero modes at each edge. The zero mode wavefunctions  $\Psi_\lambda^a$  are denoted as  $\Psi_+^a(z) = \frac{1}{\sqrt{2}} (e^{-ia\frac{\pi}{4}}, 0, 0, e^{ia\frac{\pi}{4}})^T u_+(z)$  and  $\Psi_-^a(z) = \frac{1}{\sqrt{2}} (0, e^{-ia\frac{\pi}{4}}, e^{ia\frac{\pi}{4}}, 0)^T u_-(z)$ , respectively, where  $u_a(z)$  is the envelope function with the expression given in Appendix A. Since  $[C_{ch}, S_z] = 0$ , the wavefunctions of the four zero modes can be chosen as the simultaneous eigenstates of  $C_{ch}$  and  $S_z$ :

$$C_{ch} \Psi_\lambda^a = \alpha \lambda \Psi_\lambda^a, \quad S_z \Psi_\lambda^a = \frac{1}{2} \lambda \Psi_\lambda^a. \quad (2)$$

Furthermore, there exists an emergent supersymmetry expressed as  $\gamma_+^a = \gamma_-^{a,\dagger}$ <sup>35</sup>.

When  $\Delta_s \neq 0$ , the four modes become gapped, and spontaneous magnetization develops on the edges. In this case,  $\Psi_\lambda^a$ 's remain the lowest energy states but are no longer at the zero energy, since the singlet pairing term in  $H_{1d}$  is  $-\Delta_s C_{ch}$ . Hence,  $C_{ch}$  and  $S_z$  still form a complete

set of good quantum numbers for the four modes as expressed in Eq. (2). Without loss of generality, let us consider the case of  $\Delta_s > 0$ .  $\gamma_{\lambda=a}^{a,\dagger}$  represents quasiparticle annihilation operator, since  $[H_1, \gamma_{\lambda=a}^{a,\dagger}] = -\Delta_s \gamma_{\lambda=a}^{a,\dagger}$ . The projection of the  $S_z$  operator to the edge state subspace can be expressed as  $S_z = -\frac{1}{2} a \left( \gamma_{\lambda=-a}^{a,\dagger} \gamma_{\lambda=a}^{a,\dagger} - \frac{1}{2} \right)$ , hence,  $\langle G | S_z | G \rangle = \frac{1}{4} a$  where  $|G\rangle$  is the ground state of the system. Therefore, the upper and lower edges are oppositely magnetized, carrying spontaneous magnetization along the  $\pm z$ -direction, respectively, as enforced by the  $PT$ -symmetry. Define the  $PT$  operation as  $\mathcal{S} = GPT$ , where  $G : c_\sigma(z) \rightarrow i c_\sigma(z)$  ( $\sigma = \uparrow, \downarrow$ ) is a gauge transformation.  $\mathcal{S}$  flips both  $a$  and  $\lambda$  and maintains the  $C_{ch}$  index invariant, since  $\mathcal{S}$  switches the upper and lower edges, and  $\{\mathcal{S}, S_z\} = 0$  and  $[\mathcal{S}, C_{ch}] = 0$ . As a result,  $\gamma_{\lambda=a}^{a,\dagger}$  and  $\gamma_{\lambda=-a}^{-a,\dagger}$  are related by  $\mathcal{S}$  and are the eigen-operators with the same energy. As for the case of  $\Delta_s < 0$ , the magnetization at each edge is reversed with respect to the case of  $\Delta_s > 0$ .

Next we consider the  $p \pm is$  superconductors in two dimensions. There appears a single Majorana zero mode localized at the magnetic kink on the 1D edge of this system. The corresponding BdG Hamiltonian reads

$$H_{2d} = \frac{1}{2} \int d^2 \vec{r} \psi^\dagger(\vec{r}) \left\{ \left( -\frac{\hbar^2}{2m} (\partial_y^2 + \partial_z^2) - \mu(z) \right) \tau_3 - \Delta_s(y) \sigma_2 \tau_1 - \frac{1}{k_f} (\Delta_p^y i \partial_y (i \sigma_2 \sigma_2 \tau_2) + \Delta_p^z i \partial_z (i \sigma_3 \sigma_2 \tau_1)) \right\} \psi(\vec{r}), \quad (3)$$

in which  $\vec{r} = (y, z)$ .  $\Delta_p^{y,z}$  represent the triplet pairing in the orbital components of the  $y$  and  $z$ -directions, respectively, and their corresponding  $\hat{d}$ -vectors are in parallel to the orbital directions. Again the open boundary condition is imposed along the  $z$ -direction. With a uniform  $\Delta_s(y)$ , the momentum  $k_y$  along the  $y$ -direction is a good quantum number. The Hamiltonian in Eq. (3) reduces back to Eq. (1) by setting  $k_y = 0$ , thus there are two gapped modes  $\Psi_\pm^a$  on each edge  $a$ .

At a small but nonzero  $k_y$ , the effective 1D low energy edge Hamiltonian can be obtained by the  $k \cdot p$  method, as  $H_{2d,edge}^a = -a (\Delta_s s_3 + \frac{\Delta_p^y}{k_f} k_y s_1)$ , in which  $s_i$ 's are the Pauli matrices in the basis of  $\Psi_\pm^a$  for the  $a$  edge. According to Eq. (2),  $s_3$ 's eigenstates are spin-polarized along  $\pm \hat{z}$  directions. For spatially dependent  $\Delta_s(y)$ , the edge Hamiltonian becomes

$$H_{2d,edge}^a = -a \left( \Delta_s(y) s_3 - i \frac{\Delta_p^y}{k_f} \partial_y s_1 \right). \quad (4)$$

The direction of edge magnetization is determined by the sign of  $\Delta_s(y)$ . Hence, the position where  $\Delta_s(y)$  changes sign forms a magnetic kink separating regions of opposite directions of magnetization. Alternatively,  $\Delta_s(y)$  can be viewed as the mass of the 1D superconducting spinless fermion model, therefore, a Majorana zero mode

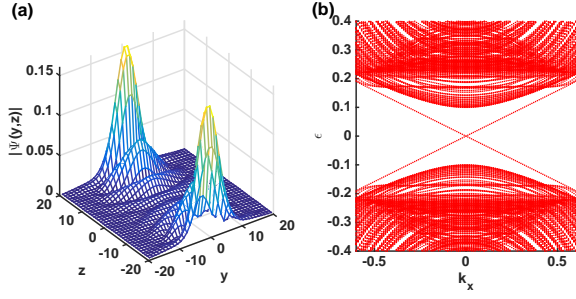


FIG. 1: (a) The probability density for one of the two zero modes of the Hamiltonian in Eq. (3). The numerical computation is carried out on a  $40 \times 40$  lattice system in the  $yz$  plane. (b) The spectrum of the Hamiltonian in Eq. (6) against  $k_x$ . In the tight binding model which is used for numerical calculations, the parameters are chosen as  $t = 1$ ,  $\mu = 0.4$ ,  $\Delta_s(y) = -0.1 \text{ sign}(y)$ , and  $\frac{\Delta_p}{\sqrt{\mu}} = 0.2$ . An open boundary condition is taken for both  $y$ - and  $z$ -directions. Due to the finite size effect, there is an energy splitting on the order of  $10^{-4}$  between the two zero modes.

arises at the magnetic kink<sup>36</sup>. The Majorana zero mode can be solved based on the low energy edge Hamiltonian in Eq. (4). For a kink with  $\text{sgn}(\Delta_s(y)) = -\lambda \text{sgn}(y)$  where  $\lambda = \pm$ , the zero mode wavefunction is  $W_\lambda^a(y, z) = \frac{1}{\sqrt{2}} (e^{i\lambda\frac{\pi}{4}} \Psi_+^a(z) + e^{-i\lambda\frac{\pi}{4}} \Psi_-^a(z)) w_\lambda(y)$ , and the envelope function reads  $w_\lambda(y) = \frac{1}{N} e^{\lambda \int_0^y dy' k_f \frac{\Delta_s(y')}{\Delta_p}}$  with  $N$  a normalization factor.

The existence of Majorana zero mode localized at the magnetic kink on the boundary is verified by numerical computations as shown in Fig. 1 (a). The calculation is performed on a finite size system based on a tight-binding model with details included in Appendix B. In Fig. 1 (a), the wavefunction mixing between the upper and lower edges is a finite size effect, leading to a small energy splitting of the two zero modes  $W_\lambda^\pm$ . In the thermodynamic limit, the two modes localized at upper and lower edges are degenerate at zero energy.

The symmetry properties of the four zero modes  $W_\lambda^a$ 's are analyzed as follows. With the presence of  $\Delta_s$ ,  $C_{ch}$  is no longer a symmetry of the zero modes, nevertheless, a new chiral operator can be chosen as  $C'_{ch} = -\sigma_3\tau_1$  which anticommutes with  $H_{2d}$  and is a symmetry for  $W_\lambda^a$ 's. When  $\Delta_s(y)$  is an odd function, the system is invariant under the operation  $M'_y = GM_y$ , where the reflection operation  $M_y$  is defined as  $M_y\psi^\dagger(y, z)M_y^{-1} = \psi^\dagger(-y, z)i\sigma_2\tau_0$ .  $C'_{ch}$  and  $M'_y$  commute and form a complete set of good quantum numbers for the four zero modes  $W_\lambda^a$ 's:

$$C'_{ch}W_\lambda^a = -a\lambda W_\lambda^a, \quad M'_yW_\lambda^a = -\lambda W_\lambda^a. \quad (5)$$

For a fixed  $\lambda$ , the  $C'_{ch}$  indices of the pair of states  $W_\lambda^\pm$  are opposite, while the  $M'_y$  eigenvalues are the same, which is the consequence of the symmetry operation  $\bar{M}_z = GM_zT$ , where  $M_z$  is the reflection operation defined as  $M_z\psi^\dagger(y, z)M_z^{-1} = \psi^\dagger(y, -z)i\sigma_3\tau_3$ .  $W_\lambda^a$  and

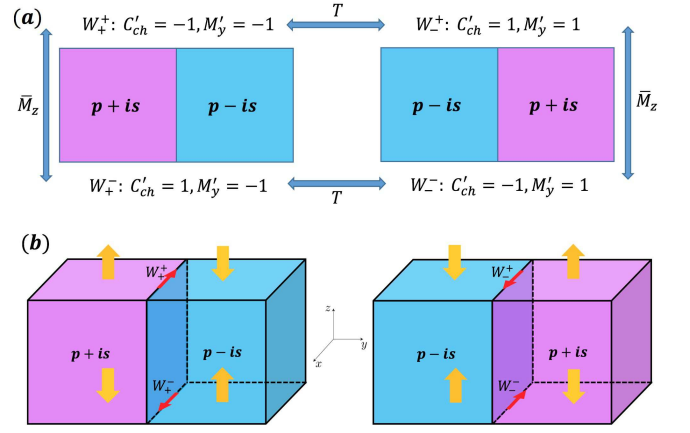


FIG. 2: (a) The relations between the  $C'_{ch}$  and the  $M'_y$  eigenvalues of the four Majorana modes  $W_\pm^{U,L}$ . (b) The directions of the propagating chiral Majorana modes along the boundaries of the interfaces between the superconducting  $p+is$  and  $p-is$  bulks.

$W_\lambda^{-a}$  are related by  $\bar{M}_z$  with opposite  $C'_{ch}$  indices and same  $M'_y$  eigenvalues, since  $\bar{M}_z$  switches the upper and lower edges, and  $[\bar{M}_z, M'_y] = 0$  and  $\{\bar{M}_z, C'_{ch}\} = 0$ . For a fixed  $a$ , both the  $C'_{ch}$  indices and the  $M'_y$  eigenvalues of the states  $W_\pm^a$  are opposite. This is due to the time reversal operation, which switches the  $p+is$  and  $p-is$  bulks and anti-commutes with both  $C'_{ch}$  and  $M'_y$ . The relations between the  $C'_{ch}$  indices and the  $M'_y$  eigenvalues of the four Majorana modes is schematically shown in Fig. 2 (a). Detailed discussions are included in Appendix C.

Now we extend the above discussions to 3D  $p \pm is$  superconductors, with the following BdG Hamiltonian

$$H_{3d} = \frac{1}{2} \int d\vec{r} \psi^\dagger(\vec{r}) \left( -\frac{\hbar^2}{2m} \nabla^2 - \mu(z) \right) \tau_3 - \Delta_s(y) \sigma_2 \tau_1 + \frac{1}{k_f} (\Delta_p^x i \partial_x \sigma_3 \tau_1 + \Delta_p^y i \partial_y \tau_2 - \Delta_p^z i \partial_z \sigma_1 \tau_1) \psi(\vec{r}). \quad (6)$$

The open boundary condition is imposed along  $z$ -direction same as before.  $H_{3d}$  reduces to the Hamiltonian in Eq. (1) when  $k_x = k_y = 0$ , and to Eq. (3) when  $k_x = 0$ .

When  $\Delta_s(y) = \Delta_s$  is a constant, the surface is uniformly spin polarized. The surface modes at  $k_x = k_y = 0$  are  $\Psi_\lambda^a$ 's as given in Eq. (2). Away from the surface  $\Gamma$ -point, the low energy surface Hamiltonian for the  $a$  boundary can be obtained by the  $k \cdot p$  method as

$$H_{\text{surf}}^a = a \left( -\Delta_s \xi_3 + \frac{1}{k_f} (\Delta_p^x k_x \xi_2 - \Delta_p^y k_y \xi_1) \right), \quad (7)$$

where  $s_j$ 's are the Pauli matrices in the basis of  $\Psi_\lambda^a$ . For the case of rotationally invariant triplet pairing, *i.e.*  $\Delta_p^j = \Delta_p$  ( $j = x, y, z$ ), the surface magnetization per unit area is evaluated as  $a \frac{k_f^2}{8\pi} r (\sqrt{1+r^2} - r)$  with  $r = \Delta_s/\Delta_p$ . Detailed calculations are included in Appendix D. Due to the surface magnetization, the spontaneous time reversal

symmetry breaking pattern (i.e. the sign of  $\Delta_s$ ) can be controlled by external magnetic field. A possible controlling scheme is that one can apply an arbitrarily small field along positive (negative)  $z$ -direction to the upper boundary of the system above superconducting transition, then  $p + is$  ( $p - is$ ) state will be favored near the upper boundary when the system is cooled down to be superconducting.

When  $\Delta_s(y)$  is an odd function, there exists chiral Majorana mode propagating along the line of the magnetic domain wall where  $\Delta_s(y)$  changes sign on the boundary of the system. We first analyze the symmetry properties of  $H_{3d}$ . Define  $C'_{ch} = GM_xTP_h$ , which satisfies  $C'_{ch}\psi^\dagger(x, y, z)C'^{-1}_{ch} = \psi^\dagger(-x, y, z)(-\sigma_3\tau_1)$ , where  $M_x$  is the reflection operation defined as  $M_x\psi^\dagger(x, y, z)M_x^{-1} = \psi^\dagger(-x, y, z)i\sigma_3\tau_3$ .  $C'_{ch}$  is the chiral operator of the system which anti-commutes with  $H_{3d}$  and reduces to  $-\sigma_3\tau_1$  when  $k_x = 0$ . The 3D extensions of  $M'_y$  and  $\bar{M}_z$  commute with  $H_{3d}$  and are symmetries of the system. The dispersion of the chiral Majorana mode can be obtained by the  $k \cdot p$  method. Assume  $\text{sgn}(\Delta_s(y)) = -\lambda \text{sgn}(y)$  with  $\lambda = \pm 1$ . Then for a fixed  $\lambda$ , there exists a Majorana zero mode  $W_\lambda^a$  with  $k_x = 0$  on boundary  $a$ . As  $k_x$  deviates from 0,  $\Delta H_{ch}(k_x) = -\frac{\Delta_x}{k_f}k_x\sigma_3\tau_1$ . As discussed before,  $W_\lambda^a$ 's are the eigenstates of  $-\sigma_3\tau_1$ , hence, the propagation direction, i.e., the chirality, is determined by the  $C'_{ch}$  index and the velocity is  $v = C'_{ch}\frac{\Delta_x}{\hbar k_f}$ . The analysis above is confirmed by numerical computations on a finite size lattice system as shown in Fig. 1 (b). The slope of the mid-gap dispersion in Fig. 1 (b) is consistent with the value of  $v$ . A schematic plot of the propagation of the Majorana modes is shown in Fig. 2 (b).

In  $p \pm is$  superconductors, spatial inhomogeneities, including the spatial variations of the external potential  $V(\vec{r})$  and the gap functions of the  $s$  and  $p$ -wave pairings, can induce spin polarizations. In the following, a Ginzburg-Landau free energy analysis is presented for the mechanism of magnetization, which holds for temperatures close to the transition temperature  $T_c$ . Denote the magnetic field as  $\vec{h}(\vec{r})$ , the singlet and triplet pairing gap functions as  $\Delta_s(\vec{r})$  and  $\Delta_p(\vec{r})$ , respectively, where an isotropic  $p$ -wave pairing is assumed, i.e.,  $\Delta_p^j = \Delta_p$  ( $j = x, y, z$ ). The free energy acquires the following terms under  $\vec{h}(\vec{r})$  as

$$\begin{aligned} \Delta F^{(3)} &= \frac{2}{3}D\epsilon_f \int d^3\vec{r} \vec{h} \cdot \text{Im}[-(\nabla\Delta_s)\Delta_p^* + \Delta_s\nabla\Delta_p^*], \\ \Delta F^{(4)} &= D \int d^3\vec{r} \vec{h} \cdot \text{Im}[(\nabla V)\Delta_s\Delta_p^* - V(\nabla\Delta_s)\Delta_p^* \\ &\quad + V\Delta_s\nabla\Delta_p^*], \end{aligned} \quad (8)$$

in which  $\epsilon_f$  is the Fermi energy,  $k_f$  is the Fermi wavevector.  $D = N_f \frac{1}{k_f} \frac{7\zeta(3)}{(8\pi)^2} \frac{1}{T_c^2}$  where  $N_f$  is the density of states at the Fermi energy,  $T_c$  is the superconducting transition temperature, and  $\zeta$  is the Riemann zeta function. The derivations to Eq. 8 are included in Appendices E and

F. Since the magnetization  $\vec{M}$  is conjugate to  $\vec{h}$ ,  $\nabla\Delta_s$ ,  $\nabla\Delta_p$  and  $\nabla V$  can all induce  $\vec{M}$ .

The first term in  $\Delta F^{(4)}$  leads to the magnetoelectric effect. The magnetization induced by the spatial variation of the external potential is given by  $\vec{M}(\vec{r}) = \chi\nabla V(\vec{r})$ , where  $\chi = D\text{Im}(\Delta_p\Delta_s^*)$ . A nonzero  $\chi$  requires the coexistence of  $\Delta_s$  and  $\Delta_p$ , and that the phase phase difference should not equal 0 and  $\pi$ , hence, both the inversion and time-reversal symmetries are broken. As analyzed before, the  $p \pm is$  pairing gap functions are energetically favored when they are nearly degenerate. In this case,  $\chi$  is nonzero and its signs are opposite for the  $p \pm is$  cases. The open boundary condition used previously corresponds to a jump of the external potential. Hence, the spin polarized surface states is a manifestation of the magnetoelectric effect. Magnetizations can also be induced by the spatial inhomogeneity of the superconducting gap functions as described in  $\Delta F^{(3)}$ . This effect is embodied in the spontaneous magnetization at the interfaces between domains with different pairing symmetries in the bulk. For the interface between  $p \pm is$  pairing domains, we find localized and spin polarized mid-gap states at the energy of  $|\Delta_p|$ , while for that of the  $\pm p + is$  pairings, such states also appear and their energy becomes  $|\Delta_s|$ . Derivations are included in Appendices G and H.

The chiral Majorana modes can be dragged and controlled by a current carrying wire placed on the surface of the system. The directions of the magnetic fields on the surface produced by the wire are antiparallel on the opposite sides of the wire, thus the induced symmetry breaking pattern ( $p + is$  or  $p - is$ ) changes across the wire when the system is cooled below  $T_c$ . As discussed previously, there exists a chiral Majorana mode on the domain wall along the wire. Such chiral Majorana mode can be dragged by translating the wire on the surface.

In summary, we have proposed that both the localized Majorana zero states and the dispersive chiral ones can be realized via the ‘‘boundary of boundary’’ method. They appear at the kinks or the boundaries of magnetization domains on edges or surfaces of the  $p \pm is$  superconductors. The boundaries of  $p \pm is$  superconductors are spontaneously magnetized, with opposite directions of magnetization for the  $p \pm is$  pairings, as a manifestation of the magnetoelectric effect. Along the 1D domain wall between the  $p \pm is$  domains on the surface, there exists a chiral Majorana mode propagating unidirectionally, which can be controlled by external magnetic field. Our discussions are relevant to the superconducting materials with competing singlet and triplet pairing orders, which apply to electric dipolar fermion systems<sup>24</sup> and possibly to  $\text{Cu}_x\text{Bi}_2\text{Se}_3$ <sup>31</sup>,  $\text{Sn}_{1-x}\text{In}_x\text{Te}$ <sup>31</sup>, and  $\text{Cd}_2\text{Re}_2\text{O}_7$ <sup>27</sup> as well.

*Acknowledgement.*— W. Y., C. X. and C. W. acknowledge the support from the NSF DMR-1410375 and AFOSR FA9550-14-1-0168. C. W. also acknowledges the support from the National Natural Science Foundation of China (11729402).

- 
- <sup>1</sup> E. Majorana, *Il Nuovo Cimento (1924-1942)* **14**, 171 (2008).
- <sup>2</sup> C. Nayak, S. H. Simon, A. Stern, M. Freedman, and S. Das Sarma, *Rev. Mod. Phys.* **80**, 1083 (2008).
- <sup>3</sup> G. Moore and N. Read, *Nuclear Physics B* **360**, 362 (1991).
- <sup>4</sup> C. Nayak and F. Wilczek, *Nuclear Physics B* **479**, 529 (1996).
- <sup>5</sup> D. A. Ivanov, *Phys. Rev. Lett.* **86**, 268 (2001).
- <sup>6</sup> A. Stern, F. von Oppen, and E. Mariani, *Phys. Rev. B* **70**, 205338 (2004).
- <sup>7</sup> A. Kitaev, *Annals of Physics* **303**, 2 (2003).
- <sup>8</sup> A. Kitaev, *Annals of Physics* **321**, 2 (2006).
- <sup>9</sup> M. Stone and S.-B. Chung, *Phys. Rev. B* **73**, 014505 (2006).
- <sup>10</sup> J. Alicea, Y. Oreg, G. Refael, F. von Oppen, and M. P. A. Fisher, *Nat. Phys.* **7**, 412 (2011).
- <sup>11</sup> B. I. Halperin, Y. Oreg, A. Stern, G. Refael, J. Alicea, and F. von Oppen, *Phys. Rev. B* **85**, 144501 (2012).
- <sup>12</sup> A. Y. Kitaev, *Phys. Uspekhi* **44**, 1 (2001).
- <sup>13</sup> N. Read and D. Green, *Phys. Rev. B* **61**, 10267 (2000).
- <sup>14</sup> L. Fu and C. L. Kane, *Phys. Rev. Lett.* **100**, 096407 (2008).
- <sup>15</sup> J. D. Sau, R. M. Lutchyn, S. Tewari, and S. Das Sarma, *Phys. Rev. Lett.* **104**, 040502 (2010).
- <sup>16</sup> S. Das Sarma, C. Nayak, and S. Tewari, *Phys. Rev. B* **73**, 220502 (2006).
- <sup>17</sup> J. C. Y. Teo and C. L. Kane, *Phys. Rev. Lett.* **104**, 046401 (2010).
- <sup>18</sup> M. Cheng, R. M. Lutchyn, V. Galitski, and S. Das Sarma, *Phys. Rev. Lett.* **103**, 107001 (2009).
- <sup>19</sup> Y. Li, D. Wang, and C. Wu, *New Journal of Physics* **15**, 085002 (2013).
- <sup>20</sup> A. C. Potter and P. A. Lee, *Phys. Rev. Lett.* **112**, 117002 (2014).
- <sup>21</sup> Y.-J. Doh, J. A. van Dam, A. L. Roest, E. P. A. M. Bakkers, L. P. Kouwenhoven, and S. D. Franceschi, *Science* **309**, 272 (2005).
- <sup>22</sup> H. H. Sun, K. W. Zhang, L. H. Hu, C. Li, G. Y. Wang, H. Y. Ma, Z. A. Xu, C. L. Gao, D. D. Guan, Y. Y. Li, C. Liu, D. Qian, Y. Zhou, L. Fu, S. C. Li, F. C. Zhang, and J. F. Jia, *Phys. Rev. Lett.* **116**, 257003 (2016).
- <sup>23</sup> Q. L. He, L. Pan, A. L. Stern, E. C. Burks, X. Che, G. Yin, J. Wang, B. Lian, Q. Zhou, E. S. Choi, K. Murata, X. Kou, Z. Chen, T. Nie, Q. Shao, Y. Fan, S. C. Zhang, K. Liu, J. Xia, K. L. Wang, *Science* **357**, 294 (2017).
- <sup>24</sup> C. Wu and J. E. Hirsch, *Phys. Rev. B* **81**, 020508 (2010).
- <sup>25</sup> L. Zhou, W. Yi and X. Cui, *arXiv:1512.09313* (2015).
- <sup>26</sup> A. Hinojosa, R. M. Fernandes, and A. V. Chubukov, *Phys. Rev. Lett.* **113**, 167001 (2014).
- <sup>27</sup> Y. Wang, and L. Fu, *Phys. Rev. Lett.* **119**, 187003 (2017).
- <sup>28</sup> S. Ryu, J. E. Moore, and A. W. W. Ludwig, *Phys. Rev. B* **85**, 045104 (2012).
- <sup>29</sup> X.-L. Qi, E. Witten, and S.-C. Zhang, *Phys. Rev. B* **87**, 134519 (2013).
- <sup>30</sup> K. Shiozaki and S. Fujimoto, *Phys. Rev. B* **89**, 054506 (2014).
- <sup>31</sup> P. Goswami and B. Roy, *Phys. Rev. B* **90**, 041301 (2014).
- <sup>32</sup> P. Goswami and A. H. Nevidomskyy, *Phys. Rev. B* **92**, 214504 (2015).
- <sup>33</sup> M. Stone and P. L. e. S. Lopes, *Phys. Rev. B* **93**, 174501 (2016).
- <sup>34</sup> A. J. Leggett, *Rev. Mod. Phys.* **47**, 331 (1975).
- <sup>35</sup> X. L. Qi, T. L. Hughes, S. Raghu, and S. C. Zhang, *Phys. Rev. Lett.* **102**, 187001 (2009).
- <sup>36</sup> A. P. Schnyder, S. Ryu, A. Furusaki, and A. W. W. Ludwig, *Phys. Rev. B* **78**, 195125 (2008).

## Appendix A: Surface states of $p \pm is$ superconductors

In this section, we solve for the surface states of a  $p + is$  superconductor.

The wavefunction can be written as  $(u_{\pm}(z)^T v_{\pm}(z)^T) e^{i(k_x x + k_y y)}$ , in which both  $u_{\pm}(z)$  and  $v_{\pm}(z)$  are two-component column vectors, and plus (minus) sign is for upper (lower) boundary. Substituting  $v_{\pm}(z)$  with  $v_{\pm}(z) = \pm i \sigma_1 u_{\pm}(z)$  in the eigen-equation, one obtains

$$\begin{aligned} & \left( \frac{\hbar^2}{2m} (-\partial_z^2 - k_f^2 + k_{\parallel}^2) \mp \frac{\Delta_p}{k_f} \partial_z \right) u_{\pm}(z) \\ & \pm \left( -\Delta_s \sigma_3 + \frac{\Delta_p}{k_f} (k_x \sigma_2 - k_y \sigma_1) \right) u_{\pm}(z) = E_s(\vec{k}_{\parallel}) u_{\pm}(z), \end{aligned} \quad (\text{A1})$$

in which  $\vec{k}_{\parallel} = (k_x, k_y)$ ,  $k_{\parallel}^2 = k_x^2 + k_y^2$ , and  $E_s(\vec{k}_{\parallel})$  is the energy of the surface state. At  $k_x = k_y = 0$  and  $\Delta_s = 0$ , the equation

$$\left( \frac{\hbar^2}{2m} (-\partial_z^2 - k_f^2 + k_{\parallel}^2) \mp \frac{\Delta_p}{k_f} \partial_z \right) u_{\pm}(z) = 0 \quad (\text{A2})$$

has two degenerate solutions as  $u_{\pm}(z) = (1 \ 0)^T u_0^{\pm}(z)$  and

$u_{\pm}(z) = (0 \ 1)^T u_0^{\pm}(z)$ , in which  $u_0^{\pm}(z)$  is given by

$$u_0^{\pm}(z) = \frac{1}{\sqrt{N(\vec{k}_{\parallel})}} \sin(\sqrt{k_f^2 - k_{\parallel}^2} z) e^{\mp \frac{m \Delta_p}{\hbar^2 \sqrt{k_f^2 - k_{\parallel}^2}} (z \pm \frac{L}{2})} \quad (\text{A3})$$

The energies of these two states will split in the presence of the term  $\pm \left( -\Delta_s \sigma_3 + \frac{\Delta_p}{k_f} (k_x \sigma_2 - k_y \sigma_1) \right) u(z)$  in Eq. (A1). The dispersion is clearly  $\pm \sqrt{\Delta_s^2 + \left( \frac{\Delta_p}{k_f} \right)^2 k_{\parallel}^2}$ .

## Appendix B: The tight binding model for numerical computations

In this section, we present the tight binding model on a lattice system which reduces to the Hamiltonian Eq. (6) in the long wavelength limit. The numerical results displayed in Fig. 1 are based on the model presented here.

A two dimensional square lattice is considered with the lattice points at  $\vec{R} = a \hat{e}_y + b \hat{e}_z$  ( $a, b \in \mathbb{Z}$ ), where  $\hat{e}_y$  (or  $\hat{e}_z$ ) is the unit vector along the  $y$  (or  $z$ )-direction. For fixed  $k_x$ , the Hamiltonian of the two dimensional tight binding model reads

$$\begin{aligned} H_t(k_x) &= \sum_{\vec{R}} \psi^{\dagger}(k_x, \vec{R}) \left[ -(\mu - k_x^2) \sigma_0 \tau_3 - \Delta_s(y) \sigma_2 \tau_1 - k_x \sigma_3 \tau_1 \right] \psi(k_x, \vec{R}) \\ &\quad - t \sum_{\vec{R}} \left[ (\psi^{\dagger}(k_x, \vec{R}) \psi(k_x, \vec{R} + \hat{e}_y) + \psi^{\dagger}(k_x, \vec{R}) \psi(k_x, \vec{R} + \hat{e}_z) - 2\psi^{\dagger}(k_x, \vec{R}) \psi(k_x, \vec{R})) + h.c. \right] \\ &\quad + \frac{1}{2i} t \frac{\Delta_p}{\sqrt{\mu}} \sum_{\vec{R}} \left[ \psi^{\dagger}(k_x, \vec{R}) (-\sigma_0 \tau_2) \psi(k_x, \vec{R} + \hat{e}_y) + \psi^{\dagger}(k_x, \vec{R}) (\sigma_1 \tau_1) \psi(k_x, \vec{R} + \hat{e}_z) + h.c. \right]. \end{aligned} \quad (\text{B1})$$

The Hamiltonian in Eq. (6) is translationally invariant along the  $x$ -direction, hence,  $k_x$  is a good quantum number. It is not hard to see that apart from an overall factor, Eq. (6) essentially describes the same system as Eq. (B1) in the long wavelength limit by setting  $-i \partial_x$  as  $k_x$  in Eq. (6).

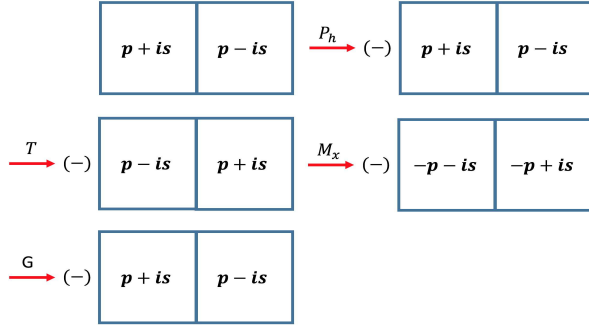
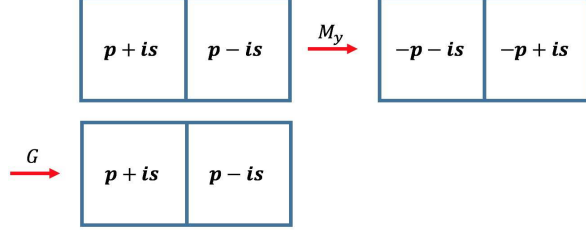
## Appendix C: Symmetry operations

In this section, we analyze the symmetries of the system and the relations between the symmetry operations. The coordinate system is chosen according to the convention denoted in Fig. 1.

### 1. $C'_{ch}$

We show that the operation  $C'_{ch} = G M_x T P_h$  defined in the main text anti-commutes with the Hamiltonian in Eq. (6) with  $\Delta_s(y)$  an odd function. The effects of the operations  $P_h, T, M_x, G$  on the system are schematically shown in Fig. 3.  $P_h$  anti-commutes with the Hamiltonian which is denoted by the overall minus sign in the figure. The triplet pairing is time reversal invariant, but the singlet component changes sign due to the factor of  $i$ . The  $s$ -wave component is invariant under the reflection operation, but the  $p$ -wave component changes sign since  $\vec{p} \cdot \vec{\sigma}$  is a pseudo-scalar. The gauge transformation reverses the sign of the pairing. As shown in Fig. 3, the composed operation  $C'_{ch}$  anti-commutes with the Hamiltonian.

It can also be explicitly checked that  $C'_{ch}$  anti-

FIG. 3: The symmetry operation  $C'_{ch} = GM_xTP_h$ .FIG. 4: The symmetry operation  $M'_y = GM_y$ .

commutes with the Hamiltonian. The action of  $C'_{ch}$  is

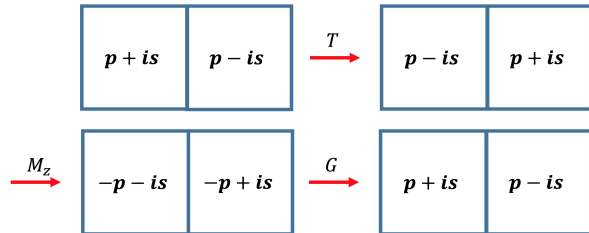
$$C'_{ch} : (x, y, z) \rightarrow (-x, y, z), (p_x, p_y, p_z) \rightarrow (-p_x, p_y, p_z);$$

$$-\sigma_3\tau_1, \quad (\text{C1})$$

in which the first and second row denote how  $C'_{ch}$  acts in the spatial and internal degrees of freedom, respectively.  $-\sigma_3\tau_1$  anti-commutes with all terms in the Hamiltonian Eq. (6) except  $-\frac{\Delta_p}{k_f}k_x\sigma_3\tau_1$ . But the spatial part of  $C'_{ch}$  reverses the sign of  $k_x$ . Hence,  $\{C'_{ch}, H\} = 0$ .

## 2. $M'_y$

We now show that the operation  $M'_y = GM_y$  defined in the main text commutes with the Hamiltonian in Eq. (6). The effects of the operations  $M_y, G$  on the system are schematically shown in Fig. 4.  $M_y$  interchanges the left and right bulks and keeps the  $s$ -wave component invariant.  $M_y$  also reverses the sign of the  $p$ -wave component since  $\vec{p} \cdot \vec{\sigma}$  is a pseudo-scalar. The gauge transformation

FIG. 5: The symmetry operation  $\bar{M}_z = GM_zT$ .

changes the sign of the pairing. Thus the operation  $M'_y$  brings the system back.

It can also be explicitly checked that  $M'_y$  commutes with the Hamiltonian. The action of  $M'_y$  is

$$M'_y : (x, y, z) \rightarrow (x, -y, z), (p_x, p_y, p_z) \rightarrow (p_x, -p_y, p_z);$$

$$-\sigma_2\tau_3. \quad (\text{C2})$$

$-\sigma_2\tau_3$  commutes with all terms in the Hamiltonian in Eq. (6) except for  $-\frac{\Delta_p}{k_f}k_y\sigma_0\tau_2$  and  $-\Delta_s(y)\sigma_2\tau_1$ . But the spatial part of  $M'_y$  reverses the sign of both these two terms. Thus  $[M'_y, H] = 0$ .

## 3. $\bar{M}_z$

In this part, we show that the operation  $\bar{M}_z = GM_zT$  commutes with  $H$  and  $M'_y$ , and anti-commutes with  $C'_{ch}$ . The effects of the operations  $T, M_z, G$  on the system are schematically shown in Fig. 5, and the combination of them keeps the system invariant. The commutation relations can be checked explicitly. The action of  $\bar{M}_z$  is

$$\bar{M}_z : (x, y, z) \rightarrow (x, y, -z), (p_x, p_y, p_z) \rightarrow (-p_x, -p_y, p_z);$$

$$\sigma_1\tau_0K. \quad (\text{C3})$$

$\sigma_1\tau_0K$  commutes with all terms in the Hamiltonian except for  $-\frac{\Delta_p}{k_f}p_x\sigma_3\tau_1$  and  $-\frac{\Delta_p}{k_f}p_y\sigma_0\tau_2$ , but the spatial part of the action of  $\bar{M}_z$  reverses the sign of  $p_x, p_y$ , thus  $[\bar{M}_z, H] = 0$ . Using the explicit expressions in Eqs. (C1,C2,C3), the relations  $\{\bar{M}_z, C'_{ch}\} = 0$  and  $[\bar{M}_z, M'_y] = 0$  can be easily checked.

## 4. $T$

In this part, we show that  $T$  switches the bulks of  $p+is$  and  $p-is$  pairings and satisfies the anti-commutation relations  $\{T, C'_{ch}\} = 0$  and  $\{T, M'_y\} = 0$ . The action of the time reversal operation is plotted in the first arrow of Fig. 5. Clearly  $T$  interchanges the left and right bulks. The explicit form of the action of  $T$  is

$$T : (x, y, z) \rightarrow (x, y, z), (p_x, p_y, p_z) \rightarrow (-p_x, -p_y, -p_z);$$

$$i\sigma_2K. \quad (\text{C4})$$

Using the expressions in Eqs. (C1,C2,C4), it can be verified that  $\{T, C'_{ch}\} = 0$ ,  $\{T, M'_y\} = 0$ .

## Appendix D: Surface magnetization of $p \pm is$ superconductors

In this section, we compute the spontaneous magnetization on the boundary of the  $p+is$  superconductor. The upper boundary is taken as an example for calculations.

The quasiparticle creation operator can be expressed as

$$\gamma_{a,\vec{k}_{\parallel}}^{\dagger} = \int dz \psi^{\dagger}(\vec{k}_{\parallel}, z) \Psi_a^+(\vec{k}_{\parallel}, z), \quad (\text{D1})$$

in which  $a = \pm$ . The second quantized form of the surface Hamiltonian is

$$H_{\text{surf}} = \frac{1}{2} \sum_{\vec{k}_{\parallel}} (\gamma_{+,\vec{k}_{\parallel}}^{\dagger} \quad \gamma_{-,\vec{k}_{\parallel}}^{\dagger}) H_{\text{surf}}(\vec{k}_{\parallel}) \begin{pmatrix} \gamma_{+,\vec{k}_{\parallel}} \\ \gamma_{-,\vec{k}_{\parallel}} \end{pmatrix}, \quad (\text{D2})$$

in which the matrix kernel  $H_{\text{surf}}(\vec{k}_{\parallel})$  is given by  $H_{\text{surf}}(k_x, k_y) = -\vec{h}(\vec{k}_{\parallel}) \cdot \vec{\xi}$ , where  $\vec{h}(\vec{k}_{\parallel}) = (\frac{\Delta_p}{k_f} k_y, -\frac{\Delta_p}{k_f} k_x, \Delta_s)^T$ ,  $\xi_i$ 's are the Pauli matrices, and  $\vec{\xi} = (\xi_1, \xi_2, \xi_3)^T$ . Due to the relation

$$\gamma_{+,\vec{k}_{\parallel}}^{\dagger} = \gamma_{-,-\vec{k}_{\parallel}}, \quad (\text{D3})$$

the Hamiltonian in Eq. (D2) can be written as

$$H_{\text{surf}} = \frac{1}{2} \sum_{\vec{k}_{\parallel}} (\gamma_{-,-\vec{k}_{\parallel}} \quad \gamma_{-,\vec{k}_{\parallel}}^{\dagger}) H_{\text{surf}}(\vec{k}_{\parallel}) \begin{pmatrix} \gamma_{-,-\vec{k}_{\parallel}}^{\dagger} \\ \gamma_{-,\vec{k}_{\parallel}} \end{pmatrix}. \quad (\text{D4})$$

In the following, we will drop the subscript “-” and simply write  $\gamma_{-,\vec{k}_{\parallel}}$  as  $\gamma_{\vec{k}_{\parallel}}$ .

Define  $a_{\vec{k}_{\parallel}}$  through the relation

$$\begin{pmatrix} \gamma_{-\vec{k}_{\parallel}}^{\dagger} \\ \gamma_{\vec{k}_{\parallel}} \end{pmatrix} = U(\hat{h}) \begin{pmatrix} a_{-\vec{k}_{\parallel}}^{\dagger} \\ a_{\vec{k}_{\parallel}} \end{pmatrix} \quad (\text{D5})$$

in which  $U(\hat{h}) = e^{-i\frac{1}{2}\xi_z\phi_h} e^{-i\frac{1}{2}\xi_y\theta_h}$ , where  $\theta_h$  and  $\phi_h$  are the polar and azimuthal angles of the vector  $\vec{h}(\vec{k}_{\parallel})$ . The surface Hamiltonian becomes diagonal in terms of  $a_{\vec{k}_{\parallel}}$  as

$$H_{\text{surf}} = -\frac{1}{2} \sqrt{\Delta_s^2 + \frac{\Delta_p^2}{k_f^2} k_{\parallel}^2} \sum_{\vec{k}_{\parallel}} (a_{-\vec{k}_{\parallel}} \quad a_{\vec{k}_{\parallel}}^{\dagger}) \xi_3 \begin{pmatrix} a_{-\vec{k}_{\parallel}}^{\dagger} \\ a_{\vec{k}_{\parallel}} \end{pmatrix}. \quad (\text{D6})$$

Projecting the spin operator in  $z$ -direction to the subspace of the surface states, one obtains

$$S^z = \frac{1}{4} \sum_{\vec{k}_{\parallel}} (\gamma_{-\vec{k}_{\parallel}} \quad \gamma_{\vec{k}_{\parallel}}^{\dagger}) \xi_3 \begin{pmatrix} \gamma_{-\vec{k}_{\parallel}}^{\dagger} \\ \gamma_{\vec{k}_{\parallel}} \end{pmatrix}. \quad (\text{D7})$$

In terms of  $a_{\vec{k}_{\parallel}}$ , the  $S_z$  operator becomes

$$S^z = \frac{1}{4} \sum_{\vec{k}_{\parallel}} (a_{-\vec{k}_{\parallel}} \quad a_{\vec{k}_{\parallel}}^{\dagger}) \Lambda(\vec{k}_{\parallel}) \cdot \vec{\xi} \begin{pmatrix} a_{-\vec{k}_{\parallel}}^{\dagger} \\ a_{\vec{k}_{\parallel}} \end{pmatrix}, \quad (\text{D8})$$

in which  $\Lambda(\vec{k}_{\parallel}) = \frac{1}{\sqrt{\Delta_s^2 + \frac{\Delta_p^2}{k_f^2} k_{\parallel}^2}} (-\frac{\Delta_p}{k_f} k_{\parallel}, 0, \Delta_s)$ .

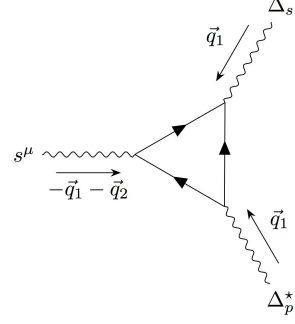


FIG. 6: The diagram contributing to  $\Delta F^{(3)}$  with the combination  $\Delta_s \Delta_p^*$ .

The ground state  $|G\rangle$  of the Hamiltonian Eq. (D6) is annihilated by  $a_{\vec{k}_{\parallel}}$ . Hence

$$M_z = \frac{1}{A} \langle G | S^z | G \rangle = \frac{1}{4} \int^{k_f} \frac{d^2 \vec{k}_{\parallel}}{(2\pi)^2} \frac{\Delta_s}{\sqrt{\Delta_s^2 + \frac{\Delta_p^2}{k_f^2} k_{\parallel}^2}}, \quad (\text{D9})$$

in which  $A$  is the area of the system. The integral is evaluated to be

$$M_z = \frac{k_f^2}{8\pi} \frac{\Delta_s}{\Delta_p} \left( \sqrt{1 + \left(\frac{\Delta_s}{\Delta_p}\right)^2} - \frac{\Delta_s}{\Delta_p} \right). \quad (\text{D10})$$

### Appendix E: Evaluation of $\Delta F^{(3)}$

There are two diagrams contributing to  $\Delta F^{(3)}$  in Eq. (8). The one with the combination  $\Delta_s \Delta_p^*$  is shown in Fig. 7. The other one with the combination  $\Delta_s^* \Delta_p$  can be obtained by taking the complex conjugate. Denote  $\mathcal{C}_\mu$  to be the value of the diagram in Fig. 6. In this section, we evaluate  $\mathcal{C}$  up to linear order of  $\vec{q}_1, \vec{q}_2, \vec{q}_3$  in the static limit. We work in the imaginary time formalism, and  $\hbar$  is set to be 1. The Fermi energy and Fermi wave vector are denoted as  $\epsilon_f$  and  $k_f$ .

The expression for  $\mathcal{C}_\mu$  is

$$\begin{aligned}
C_\mu &= \int \frac{d^3\vec{k}}{(2\pi)^3} \frac{1}{\beta} \sum_{i\omega_n} \text{Tr} \left[ \frac{1}{-i\omega_n - \xi_{\vec{k}}} i\sigma_2 \frac{1}{i\omega_n - \xi_{-\vec{k}-\vec{q}_2}} \frac{1}{2} \sigma_\mu \frac{1}{i\omega_n - \xi_{-\vec{k}+\vec{q}_1}} \frac{1}{k_f} (\vec{k} - \frac{\vec{q}_1}{2}) \cdot \vec{\sigma} i\sigma_2 \right] \\
&= \frac{1}{k_f} \int \frac{d^3\vec{k}}{(2\pi)^3} \frac{1}{\beta} \sum_{i\omega_n} (k_\mu - \frac{q_{1\mu}}{2}) \frac{(-i\omega_n + \xi_{\vec{k}})(i\omega_n + \xi_{\vec{k}+\vec{q}_2})(i\omega_n + \xi_{\vec{k}-\vec{q}_1})}{(\omega_n^2 + \xi_{\vec{k}}^2)(\omega_n^2 + \xi_{\vec{k}+\vec{q}_2}^2)(\omega_n^2 + \xi_{\vec{k}-\vec{q}_1}^2)}. \tag{E1}
\end{aligned}$$

Denote  $C_\mu^{(0)}$  as the  $\vec{q}_1 = \vec{q}_2 = \vec{q}_3 = 0$  term,  $C_\mu^{(1)}$  as the linear in  $\vec{q}_1$  term, and  $C_\mu^{(2)}$  as the linear in  $\vec{q}_2$  term of Eq. (E1). We obtain

$$C_\mu^{(0)} = \frac{1}{k_f} \int \frac{d^3\vec{k}}{(2\pi)^3} \frac{1}{\beta} \sum_{i\omega_n} k_\mu \frac{i\omega_n + \xi_{\vec{k}}}{(\omega_n^2 + \xi_{\vec{k}}^2)^2} = 0, \tag{E2}$$

$$\begin{aligned}
C_\mu^{(1)} &= \frac{1}{k_f} \int \frac{d^3\vec{k}}{(2\pi)^3} \frac{1}{\beta} \sum_{i\omega_n} k_\mu v_{\vec{k}} \hat{k} \cdot \vec{q}_1 \frac{(i\omega_n + \xi_{\vec{k}})^2}{(\omega_n^2 + \xi_{\vec{k}}^2)^3} \\
&= \frac{1}{3} v_f q_{1\mu} N_f \int d\epsilon \frac{1}{\beta} \sum_{i\omega_n} \frac{\epsilon^2 - \omega_n^2}{(\omega_n^2 + \epsilon^2)^3}, \tag{E3}
\end{aligned}$$

$$\begin{aligned}
C_\mu^{(2)} &= -\frac{1}{k_f} \int \frac{d^3\vec{k}}{(2\pi)^3} \frac{1}{\beta} \sum_{i\omega_n} k_\mu v_{\vec{k}} \hat{k} \cdot \vec{q}_2 \frac{(i\omega_n + \xi_{\vec{k}})^2}{(\omega_n^2 + \xi_{\vec{k}}^2)^3} \\
&= -\frac{1}{3} v_f q_{2\mu} N_f \int d\epsilon \frac{1}{\beta} \sum_{i\omega_n} \frac{\epsilon^2 - \omega_n^2}{(\omega_n^2 + \epsilon^2)^3}. \tag{E4}
\end{aligned}$$

Denote  $C^{(i)}$  ( $i = 1, 2$ ) to be the coefficient of  $q_{i\mu}$  in  $C_\mu^{(i)}$ . Using

$$\begin{aligned}
\int d\epsilon \frac{1}{\beta} \sum_{i\omega_n} \frac{\epsilon^2}{(\omega_n^2 + \epsilon^2)^3} &= \frac{1}{3} \int d\epsilon \frac{1}{\beta} \sum_{i\omega_n} \frac{\omega_n^2}{(\omega_n^2 + \epsilon^2)^3} \\
&= \frac{1}{4} \frac{7\zeta(3)}{(8\pi)^2} \frac{1}{T^2}, \tag{E5}
\end{aligned}$$

we obtain

$$-C^{(1)} = C^{(2)} = \frac{1}{6} N_f v_f \frac{7\zeta(3)}{(8\pi)^2} \frac{1}{T^2}. \tag{E6}$$

When the system is close to the superconducting transition point, we can set  $T = T_c$ . The diagram in Fig. 6 represents six terms in the  $Trln$ -expansion of the free energy. Since Fig. 6 is a third order term, there is an additional  $\frac{1}{3}$  factor. Combing these together, we arrive at the expression of  $\Delta F^{(3)}$ .

#### Appendix F: Evaluation of $\Delta F^{(4)}$

There are six diagrams contributing to  $\Delta F^{(4)}$  in Eq. (8). Three of them with the combination  $\Delta_s \Delta_p^*$  are shown in Fig. 7. The other three with the combination  $\Delta_s^* \Delta_p$  can be obtained by taking the complex conjugate. Let  $\mathcal{D}_\mu^{a,b,c}$  be the values of the diagrams (a, b, c) in Fig. 7, respectively. In this section, we evaluate  $\mathcal{D}_\mu^{a,b,c}$  up to linear order of  $\vec{q}_1, \vec{q}_2, \vec{q}_3$  in the static limit.

First consider the diagram Fig. 7 (a). The expression for  $\mathcal{D}_\mu^a$  is

$$\begin{aligned}
\mathcal{D}_\mu^a &= \int \frac{d^3\vec{k}}{(2\pi)^3} \frac{1}{\beta} \sum_{i\omega_n} \text{Tr} \left[ \frac{1}{-i\omega_n - \xi_{\vec{k}}} i\sigma_2 \frac{1}{i\omega_n - \xi_{-\vec{k}-\vec{q}_2}} \frac{1}{i\omega_n - \xi_{-\vec{k}-\vec{q}_2-\vec{q}_3}} \frac{1}{2} \sigma_\mu \frac{1}{i\omega_n - \xi_{-\vec{k}+\vec{q}_1}} \frac{1}{k_f} (\vec{k} - \frac{\vec{q}_1}{2}) \cdot \vec{\sigma} i\sigma_2 \right] \\
&= -\int \frac{d^3\vec{k}}{(2\pi)^3} \frac{1}{\beta} \sum_{i\omega_n} \frac{1}{k_f} (k_\mu - \frac{q_{1\mu}}{2}) \frac{(-i\omega_n + \xi_{\vec{k}})(i\omega_n + \xi_{\vec{k}+\vec{q}_2})(i\omega_n + \xi_{\vec{k}+\vec{q}_2+\vec{q}_3})(i\omega_n + \xi_{\vec{k}-\vec{q}_1})}{(\omega_n^2 + \xi_{\vec{k}}^2)(\omega_n^2 + \xi_{\vec{k}+\vec{q}_2}^2)(\omega_n^2 + \xi_{\vec{k}+\vec{q}_2+\vec{q}_3}^2)(\omega_n^2 + \xi_{\vec{k}-\vec{q}_1}^2)}, \tag{F1}
\end{aligned}$$

in which  $\xi_{\vec{k}} = \frac{k^2}{2m} - \epsilon_f$ ,  $\frac{1}{2}\sigma_\mu$  is the vertex for the spin operator,  $i\sigma_2$  is the vertex for the singlet pairing, and  $\frac{1}{k_f}(\vec{k} - \frac{\vec{q}_1}{2}) \cdot \vec{\sigma} i\sigma_2$  is the vertex for the triplet pairing.

Denote  $\mathcal{D}_\mu^{a(0,1,2,3)}$  to be the  $\vec{q}_1 = \vec{q}_2 = \vec{q}_3 = 0$  term, the linear in  $\vec{q}_1$  term, the linear in  $\vec{q}_2$  term, and the linear in

$\vec{q}_3$  term of Eq. (F1), respectively.

For  $\mathcal{D}_\mu^{a(0)}$ , we obtain

$$\mathcal{D}_\mu^{a(0)} = -\frac{1}{k_f} \int \frac{d^3\vec{k}}{(2\pi)^3} \frac{1}{\beta} \sum_{i\omega_n} k_\mu \frac{(i\omega_n + \xi_{\vec{k}})^2}{(\omega_n^2 + \xi_{\vec{k}}^2)^3} = 0, \tag{F2}$$

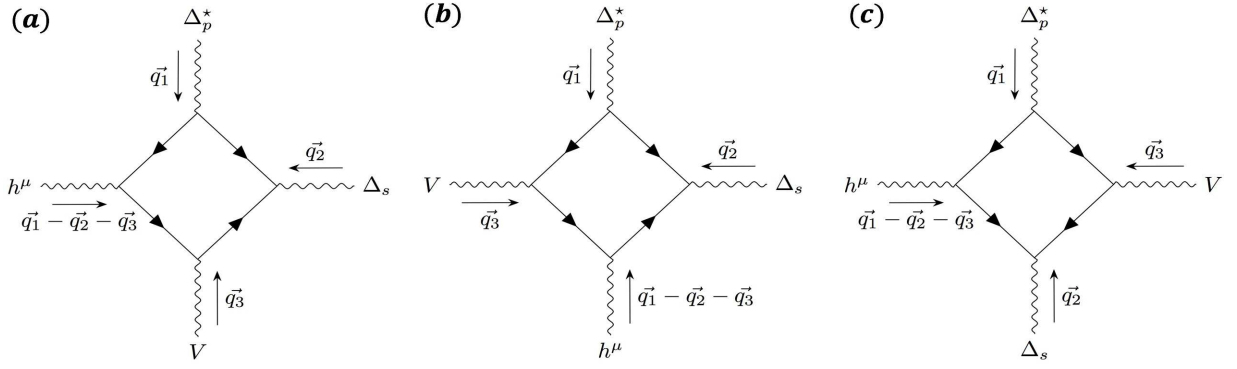


FIG. 7: The three diagrams contributing to  $\Delta F^{(4)}$  with the combination  $\Delta_s \Delta_p^*$ .

due to the rotational invariance of the dispersion  $\xi_{\vec{k}}$ .

For  $\mathcal{D}_\mu^{a(1)}$ , up to linear order in  $\vec{q}_1$ , we obtain

$$\mathcal{D}_\mu^{a(1)} = \mathcal{D}_\mu^{a(1),1} + \mathcal{D}_\mu^{a(1),2}, \quad (\text{F3})$$

in which

$$\begin{aligned} \mathcal{D}_\mu^{a(1),1} &= -\frac{1}{k_f} \int \frac{d^3 \vec{k}}{(2\pi)^3} \frac{1}{\beta} \sum_{i\omega_n} k_\mu v_k \hat{k} \cdot \vec{q}_1 \frac{(i\omega_n + \xi_{\vec{k}})^3}{(\omega_n^2 + \xi_{\vec{k}}^2)^3} \\ &= -\frac{1}{3} \frac{q_{1\mu}}{mk_f} \int \frac{d^3 \vec{k}}{(2\pi)^3} \frac{1}{\beta} \sum_{i\omega_n} k^2 \frac{(i\omega_n + \xi_{\vec{k}})^3}{(\omega_n^2 + \xi_{\vec{k}}^2)^3}, \end{aligned} \quad (\text{F4})$$

$$\mathcal{D}_\mu^{a(1),2} = \frac{q_{1\mu}}{k_f} \int \frac{d^3 \vec{k}}{(2\pi)^3} \frac{1}{\beta} \sum_{i\omega_n} \frac{(i\omega_n + \xi_{\vec{k}})^2}{(\omega_n^2 + \xi_{\vec{k}}^2)^3}. \quad (\text{F5})$$

To the lowest order in the expansion of  $\frac{1}{\beta\epsilon_f}$ , we can use the approximations  $\int \frac{d^3 \vec{k}}{(2\pi)^3} = N_f \int d\epsilon (1 + \frac{\epsilon}{2\epsilon_f})$  and  $k = k_f + \frac{\xi_{\vec{k}}}{v_f}$ , where  $N_f$  is the density of states at Fermi energy. Then one obtains

$$\mathcal{D}_\mu^{a(1),1} = -N_f \frac{q_{1,\mu}}{k_f} \int d\epsilon \frac{1}{\beta} \sum_{i\omega_n} \frac{\epsilon^2(\epsilon^2 - 3\omega_n^2)}{(\omega_n^2 + \epsilon^2)^4}, \quad (\text{F6})$$

$$\mathcal{D}_\mu^{a(1),2} = \frac{1}{2} N_f \frac{q_{1\mu}}{k_f} \int d\epsilon \frac{1}{\beta} \sum_{i\omega_n} \frac{\epsilon^2 - \omega_n^2}{(\omega_n^2 + \epsilon^2)^2}. \quad (\text{F7})$$

For  $\mathcal{D}_\mu^{a(2)}$  and  $\mathcal{D}_\mu^{a(3)}$ , the procedure of the evaluation is similar. Up to linear order in  $\vec{q}_2$  and  $\vec{q}_3$ , we obtain,

$$\mathcal{D}_\mu^{a(2)} = 2N_f \frac{q_{2\mu}}{k_f} \int d\epsilon \frac{1}{\beta} \sum_{i\omega_n} \frac{\epsilon^2(\epsilon^2 - 3\omega_n^2)}{(\omega_n^2 + \epsilon^2)^4}, \quad (\text{F8})$$

$$\mathcal{D}_\mu^{a(3)} = N_f \frac{q_{3\mu}}{k_f} \int d\epsilon \frac{1}{\beta} \sum_{i\omega_n} \frac{\epsilon^2(\epsilon^2 - 3\omega_n^2)}{(\omega_n^2 + \epsilon^2)^4}. \quad (\text{F9})$$

Next consider the diagram Fig. 7 (b). The expression for  $\mathcal{D}_\mu^b$  is

$$\begin{aligned} \mathcal{D}_\mu^b &= \int \frac{d^3 \vec{k}}{(2\pi)^3} \frac{1}{\beta} \sum_{i\omega_n} \text{Tr} \left[ \frac{1}{-i\omega_n - \xi_{\vec{k}}} i\sigma_2 \frac{1}{i\omega_n - \xi_{-\vec{k} - \vec{q}_2}} \frac{1}{2} \sigma_\mu \frac{1}{i\omega_n - \xi_{-\vec{k} + \vec{q}_1 + \vec{q}_3}} \frac{1}{i\omega_n - \xi_{-\vec{k} + \vec{q}_1}} \frac{1}{k_f} (\vec{k} - \frac{\vec{q}_1}{2}) \cdot \vec{\sigma} i\sigma_2 \right] \\ &= - \int \frac{d^3 \vec{k}}{(2\pi)^3} \frac{1}{\beta} \sum_{i\omega_n} \frac{1}{k_f} \left( k_\mu - \frac{q_{1\mu}}{2} \right) \frac{(-i\omega_n + \xi_{\vec{k}})(i\omega_n + \xi_{\vec{k} + \vec{q}_2})(i\omega_n + \xi_{-\vec{k} - \vec{q}_1 - \vec{q}_3})(i\omega_n + \xi_{-\vec{k} - \vec{q}_1})}{(\omega_n^2 + \xi_{\vec{k}}^2)(\omega_n^2 + \xi_{\vec{k} + \vec{q}_2}^2)(\omega_n^2 + \xi_{-\vec{k} - \vec{q}_1 - \vec{q}_3}^2)(\omega_n^2 + \xi_{-\vec{k} - \vec{q}_1}^2)}. \end{aligned} \quad (\text{F10})$$

Denote  $\mathcal{D}_\mu^{b(0,1,2,3)}$  to be the  $\vec{q}_1 = \vec{q}_2 = \vec{q}_3 = 0$  term, the linear in  $\vec{q}_1$  term, the linear in  $\vec{q}_2$  term, and the linear in  $\vec{q}_3$  term of Eq. (F10), respectively. The evaluations are

similar to  $\mathcal{D}_\mu^a$ . The results are

$$\mathcal{D}_\mu^{b(0)} = 0, \quad (\text{F11})$$

$$\begin{aligned} \mathcal{D}_\mu^{b(1)} &= -2N_f \frac{q_{1\mu}}{k_f} \int d\epsilon \frac{1}{\beta} \sum_{i\omega_n} \frac{\epsilon^2(\epsilon^2 - 3\omega_n^2)}{(\omega_n^2 + \epsilon^2)^4} \\ &\quad + \frac{1}{2} N_f \frac{q_{1\mu}}{k_f} \int d\epsilon \frac{1}{\beta} \sum_{i\omega_n} \frac{\epsilon^2 - \omega_n^2}{(\omega_n^2 + \epsilon^2)^3}, \quad (\text{F12}) \end{aligned} \quad \mathcal{D}_\mu^{b(3)} = -N_f \frac{q_{3\mu}}{k_f} \int d\epsilon \frac{1}{\beta} \sum_{i\omega_n} \frac{\epsilon^2(\epsilon^2 - 3\omega_n^2)}{(\omega_n^2 + \epsilon^2)^4}. \quad (\text{F14})$$

$$\mathcal{D}_\mu^{b(2)} = N_f \frac{q_{2\mu}}{k_f} \int d\epsilon \frac{1}{\beta} \sum_{i\omega_n} \frac{\epsilon^2(\epsilon^2 - 3\omega_n^2)}{(\omega_n^2 + \epsilon^2)^4}, \quad (\text{F13})$$

Finally we consider the diagram Fig. 7 (c). The expression for  $\mathcal{D}_\mu^c$  is

$$\begin{aligned} \mathcal{D}_\mu^b &= \int \frac{d^3\vec{k}}{(2\pi)^3} \frac{1}{\beta} \sum_{i\omega_n} \text{Tr} \left[ \frac{1}{-i\omega_n - \xi_{\vec{k}}} \frac{1}{-i\omega_n - \xi_{\vec{k}+\vec{q}_3}} i\sigma_2 \frac{1}{i\omega_n - \xi_{-\vec{k}-\vec{q}_2-\vec{q}_3}} \frac{1}{2} \sigma_\mu \frac{1}{i\omega_n - \xi_{-\vec{k}+\vec{q}_1}} \frac{1}{k_f} (\vec{k} - \frac{\vec{q}_1}{2}) \cdot \vec{\sigma} i\sigma_2 \right] \\ &= -\frac{1}{k_f} \int \frac{d^3\vec{k}}{(2\pi)^3} \frac{1}{\beta} \sum_{i\omega_n} \frac{1}{k_f} (k_\mu - \frac{q_{1\mu}}{2}) \frac{(-i\omega_n + \xi_{\vec{k}})(-i\omega_n + \xi_{\vec{k}+\vec{q}_3})(i\omega_n + \xi_{\vec{k}+\vec{q}_2+\vec{q}_3})(i\omega_n + \xi_{\vec{k}-\vec{q}_1})}{(\omega_n^2 + \xi_{\vec{k}}^2)(\omega_n^2 + \xi_{\vec{k}+\vec{q}_3}^2)(\omega_n^2 + \xi_{\vec{k}+\vec{q}_2+\vec{q}_3}^2)(\omega_n^2 + \xi_{\vec{k}-\vec{q}_1}^2)}. \quad (\text{F15}) \end{aligned}$$

Denote  $\mathcal{D}_\mu^{c(0,1,2,3)}$  to be the  $\vec{q}_1 = \vec{q}_2 = \vec{q}_3 = 0$  term, the linear in  $\vec{q}_1$  term, the linear in  $\vec{q}_2$  term, and the linear in  $\vec{q}_3$  term of Eq. (F15), respectively. The results are

$$\mathcal{D}_\mu^{c(0)} = 0, \quad (\text{F16})$$

$$\begin{aligned} \mathcal{D}_\mu^{c(1)} &= -N_f \frac{q_{1\mu}}{k_f} \int d\epsilon \frac{1}{\beta} \sum_{i\omega_n} \frac{\epsilon^2}{(\omega_n^2 + \epsilon^2)^3} \\ &\quad + \frac{1}{2} N_f \frac{q_{1\mu}}{k_f} \int d\epsilon \frac{1}{\beta} \sum_{i\omega_n} \frac{1}{(\omega_n^2 + \epsilon^2)^2}, \quad (\text{F17}) \end{aligned}$$

$$\mathcal{D}_\mu^{c(2)} = N_f \frac{q_{2\mu}}{k_f} \int d\epsilon \frac{1}{\beta} \sum_{i\omega_n} \frac{\epsilon^2}{(\omega_n^2 + \epsilon^2)^3}, \quad (\text{F18})$$

$$\mathcal{D}_\mu^{c(3)} = 2N_f \frac{q_{3\mu}}{k_f} \int d\epsilon \frac{1}{\beta} \sum_{i\omega_n} \frac{\epsilon^2}{(\omega_n^2 + \epsilon^2)^3}. \quad (\text{F19})$$

Define  $D^{(i)}$  ( $i = 1, 2, 3$ ) as the coefficient of  $q_{i\mu}$  in  $\mathcal{D}_\mu^{a(i)} + \mathcal{D}_\mu^{b(i)} + \mathcal{D}_\mu^{c(i)}$ . We obtain

$$D^{(1)} = N_f \frac{1}{k_f} \int d\epsilon \frac{1}{\beta} \sum_{i\omega_n} \frac{-\omega_n^4 - 5\epsilon^4 + 18\omega_n^2\epsilon^2}{2(\omega_n^2 + \epsilon^2)^4} \quad (\text{F20})$$

$$D^{(2)} = N_f \frac{1}{k_f} \int d\epsilon \frac{1}{\beta} \sum_{i\omega_n} \frac{-4\omega_n^2\epsilon^2}{(\omega_n^2 + \epsilon^2)^4}, \quad (\text{F21})$$

$$D^{(3)} = 2N_f \frac{1}{k_f} \int d\epsilon \frac{1}{\beta} \sum_{i\omega_n} \frac{\epsilon^2}{(\omega_n^2 + \epsilon^2)^3}. \quad (\text{F22})$$

Using

$$\begin{aligned} \int d\epsilon \frac{1}{\beta} \sum_{i\omega_n} \frac{\epsilon^4}{(\omega_n^2 + \epsilon^2)^4} &= \int d\epsilon \frac{1}{\beta} \sum_{i\omega_n} \frac{\epsilon^2\omega_n^2}{(\omega_n^2 + \epsilon^2)^4} \\ &= \frac{1}{5} \int d\epsilon \frac{1}{\beta} \sum_{i\omega_n} \frac{\omega_n^4}{(\omega_n^2 + \epsilon^2)^4} \\ &= \frac{7\zeta(3)}{8^3\pi^2} \frac{1}{T^2}, \quad (\text{F23}) \end{aligned}$$

one arrives at

$$D^{(1)} = -D^{(2)} = D^{(3)} = \frac{1}{2} N_f \frac{1}{k_f} \frac{7\zeta(3)}{8^2\pi^2} \frac{1}{T^2}. \quad (\text{F24})$$

When the system is close to the superconducting transition point, we can set  $T = T_c$ . Each diagram in Fig. 7 represents eight terms in the  $Tr \ln$ -expansion of the free energy. Since Fig. 7 is a fourth order term, there is an additional  $\frac{1}{4}$  factor. Combing these together, we arrive at the expression of  $\Delta F^{(4)}$ .

### Appendix G: Gapped surface states at the interface of superconducting $p + is$ and $p - is$ bulks

In this section, we solve for the surface states at the interface of superconducting  $p + is$  and  $p - is$  bulks. We consider the surface  $\Gamma$ -point, i.e.  $k_x = k_y = 0$ . The surface spectrum has a gap equal to  $\Delta_p$ .

For convenience, in this section, we use a coordinate system, such that the interface lies in the  $xy$  plane, which is different from what is chosen in Fig. 2. The spatial distribution of the singlet pairing component is taken as  $\Delta_s(z) = \Delta_s$  at  $z < 0$  and  $\Delta_s(z) = -\Delta_s$  at  $z > 0$ , where  $\Delta_s$  is assumed to be positive. At the surface  $\Gamma$ -point, the

eigen-equation is

$$\begin{aligned} \left(\frac{\hbar^2}{2m}(-\partial_z^2 - k_f^2)\tau_3 + \frac{\Delta_p}{k_f}(-i\partial_z)\sigma_1\tau_1 - \Delta_s(z)\sigma_2\tau_1\right)\Psi(z) \\ = \epsilon\Psi(z), \end{aligned} \quad (\text{G1})$$

in which  $\epsilon$  is the energy of the surface state. The boundary conditions are  $\Psi(z \rightarrow \pm\infty) \rightarrow 0$ ,  $\Psi(z \rightarrow 0+) = \Psi(z \rightarrow 0-)$ , and  $\partial_z\Psi(z \rightarrow 0+) = \partial_z\Psi(z \rightarrow 0-)$ . Plugging the trial wavefunction  $\Psi(z) = \Phi e^{ik_z z}$  into Eq. (G1), we obtain

$$\left(\frac{\hbar^2}{2m}(k_z^2 - k_f^2)\tau_3 + \frac{\Delta_p}{k_f}k_z\sigma_1\tau_1 - \Delta_s(z)\sigma_2\tau_1 - \epsilon\right)\Phi = 0, \quad (\text{G2})$$

in which  $+$  ( $-$ ) is for  $z < 0$  ( $z > 0$ ).

Eq. (G2) can be factorized into two independent equations in the  $S_z = \pm\frac{1}{2}$  sectors. In the following, we consider the  $S_z = \frac{1}{2}$  sector. The  $S_z = -\frac{1}{2}$  sector can be solved similarly. In the weak pairing limit, i.e.,  $\Delta_s, \Delta_p \ll \frac{\hbar^2 k_f^2}{2m}$ , the momentum  $k_z$  can be approximated as  $k_z = k_f(\eta - i\nu\xi)$ , in which  $\nu = 1$  when  $z < 0$  and  $\nu = -1$  when  $z > 0$ , and  $\eta = \pm 1$ .  $\xi$  is positive due to the boundary condition  $\Psi(z \rightarrow \pm\infty) \rightarrow 0$ . For each  $(\nu, \eta)$ , there is a solution  $\Phi_{\nu, \eta}$ , as

$$\Phi_{\nu, \eta} = \begin{pmatrix} \eta\Delta_p + i\nu\Delta_s \\ i\nu\eta\sqrt{\Delta_p^2 + \Delta_s^2 - \epsilon^2 + \epsilon} \end{pmatrix}, \quad (\text{G3})$$

with the corresponding  $\xi_{\nu, \eta}$  given by  $\xi_{\nu, \eta} = \frac{\sqrt{\Delta_p^2 + \Delta_s^2 - \epsilon^2}}{2}$ . Then the wavefunction  $\Psi(z)$  is given by

$$\Psi(z) = \sum_{\nu=\pm 1, \eta=\pm 1} C_{\nu, \eta} \Phi_{\nu, \eta}^\dagger e^{i\eta k_f z} e^{\nu \frac{\sqrt{\Delta_p^2 + \Delta_s^2 - \epsilon^2}}{2} z} \Theta(-\nu z), \quad (\text{G4})$$

in which  $\Theta$  is the step function defined by  $\Theta(x) = 1$  when  $x > 0$  and  $\Theta(x) = 0$  when  $x < 0$ .

Plugging Eq. (G4) into the boundary conditions at  $z = 0$ , i.e.,  $\Psi(z \rightarrow 0+) = \Psi(z \rightarrow 0-)$  and  $\partial_z\Psi(z \rightarrow 0+) = \partial_z\Psi(z \rightarrow 0-)$ , we obtain

$$\det \begin{pmatrix} \{\Phi_{\nu, \eta}\} \\ \{\eta\Phi_{\nu, \eta}\} \end{pmatrix} = 0, \quad (\text{G5})$$

in which  $\{\Phi_{\nu, \eta}\}$  is the abbreviation of the  $2 \times 4$  matrix  $\{\Phi_{+,+}^\dagger, \Phi_{+,-}^\dagger, \Phi_{-,+}^\dagger, \Phi_{-,-}^\dagger\}$ , and similar for  $\{\eta\Phi_{\nu, \eta}\}$ . The solution of Eq. (G5) is

$$\epsilon = \Delta_p, \quad (\text{G6})$$

with a two-fold degeneracy. The wavefunctions are given by

$$\Psi_\pm^\dagger(z) = \frac{1}{\sqrt{\mathcal{N}}} \begin{pmatrix} 1 \\ 0 \\ 0 \\ \pm 1 \end{pmatrix} e^{\pm i k_f z} e^{-\frac{\Delta_p}{2k_f}|z|}. \quad (\text{G7})$$

For the  $S_z = -\frac{1}{2}$  sector, there are two solutions with  $\epsilon = -\Delta_p$ , which are given by

$$\Psi_\mp^\dagger(z) = \frac{1}{\sqrt{\mathcal{N}}} \begin{pmatrix} 0 \\ \pm 1 \\ 1 \\ 0 \end{pmatrix} e^{\mp i k_f z} e^{-\frac{\Delta_s}{2k_f}|z|}. \quad (\text{G8})$$

## Appendix H: Gapped surface states at the interface of the superconducting $p + is$ and $-p + is$ bulks

In this section, we consider the surface states at the interface of superconducting  $p + is$  and  $-p + is$  bulks. We show that the surface spectrum has a gap which is equal to  $\Delta_s$ .

The coordinate system is chosen such that the interface is within the  $xy$ -plane. The singlet component is spatially uniform, and the triplet component is taken as  $\Delta_p(z) = \Delta_p$  when  $z < 0$  and  $\Delta_p(z) = -\Delta_p$  when  $z > 0$ , where  $\Delta_p$  is assumed to be positive. For simplicity, we consider the surface  $\Gamma$ -point. The eigen-equation is

$$\begin{aligned} \left(\frac{\hbar^2}{2m}(-\partial_z^2 - k_f^2)\tau_3 + \frac{\Delta_p(z)}{k_f}(-i\partial_z)\sigma_1\tau_1 - \Delta_s\sigma_2\tau_1\right)\Psi(z) \\ = \epsilon\Psi(z), \end{aligned} \quad (\text{H1})$$

with the boundary conditions  $\Psi(z \rightarrow \pm\infty) \rightarrow 0$ ,  $\Psi(z \rightarrow 0+) = \Psi(z \rightarrow 0-)$ , and  $\partial_z\Psi(z \rightarrow 0+) = \partial_z\Psi(z \rightarrow 0-)$ .

Again Eq. (H1) can be factorized into the  $S_z = \pm\frac{1}{2}$  factors. The procedure for obtaining the surface states is exactly similar as in the former section. Here we summarize the results. The two wavefunctions with  $\epsilon = -\Delta_s$  are

$$\Psi_\pm^\dagger(z) = \frac{1}{\sqrt{\mathcal{N}}} \begin{pmatrix} 1 \\ 0 \\ 0 \\ i \end{pmatrix} e^{\pm i k_f z} e^{-\frac{\Delta_p}{2k_f}|z|}, \quad (\text{H2})$$

and the two wavefunctions with  $\epsilon = \Delta_s$  are

$$\Psi_\mp^\dagger(z) = \frac{1}{\sqrt{\mathcal{N}}} \begin{pmatrix} 0 \\ -i \\ 1 \\ 0 \end{pmatrix} e^{\mp i k_f z} e^{-\frac{\Delta_p}{2k_f}|z|}. \quad (\text{H3})$$